ELSEVIER

materialstoday
BIO

materialstoday

Photo-degradable, tough and highly stretchable hydrogels

Rita G. Fonseca [a], Francesco De Bon [a], Patrícia Pereira [a,b], Francisca M. Carvalho [c], Marta Freitas [c], Mahmoud Tavakoli [c], Arménio C. Serra [a], Ana C. Fonseca [a], Jorge F.J. Coelho [a,*]

[a] *CEMMPRE - Department of Chemical Engineering, University of Coimbra, 3030-790, Coimbra, Portugal*
[b] *IPN – Instituto Pedro Nunes, Rua Pedro Nunes, 3030-199, Coimbra, Portugal*
[c] *ISR - Institute of Systems and Robotics, University of Coimbra, 3030-194, Coimbra, Portugal*

ARTICLE INFO

ABSTRACT

We present for the first time highly stretchable and tough hydrogels with controlled light-triggered photo-degradation. A double-network of alginate/polyacrylamide (PAAm) is formed by using covalently and ionically crosslinked subnetworks. The ionic Ca^{2+} alginate interpenetrates a PAAm network covalently crosslinked by a bifunctional acrylic crosslinker containing the photodegradable *o*-nitrobenzyl (ONB) core instead of the commonly used methylene bisacrylamide (MBAA). Remarkably, due to the developed protocol, the change of the crosslinker did not affect the hydrogel's mechanical properties. The incorporation of photosensitive components in hydrogels allows external temporal control of their properties and tuneable degradation. Cell viability and cell proliferation assays revealed that hydrogels and their photodegradation products are not cytotoxic to the NIH3T3 cell line. In one example of application, we used these hydrogels for bio-potential acquisition in wearable electrocardiography. Surprisingly, these hydrogels showed a lower skin-electrode impedance, compared to the common medical grade Ag/AgCl electrodes. This work lays the foundation for the next generation of tough and highly stretchable hydrogels that are environmentally friendly and can find applications in a variety of fields such as health, electronics, and energy, as they combine excellent mechanical properties with controlled degradation.

1. Introduction

Hydrogels are soft and highly-hydrated materials, composed of a crosslinked three-dimensional (3D) network of hydrophilic polymer chains, capable of swelling and retaining large amounts of water in their network structure, without dissolving [1,2]. Due to their ability to absorb water, good biocompatibility, and similarity to human tissues, hydrogels are widely used for various biomedical applications, including tissue engineering [3], drug delivery [4], biosensors [5], wearable electrodes for biomonitoring [6], printed and stretchable batteries [7], and supercapacitors [8]. However, most hydrogels are very brittle (fracture energy $\sim 10 \, J \, m^{-2}$), due to the high water content in the network, which reduces the toughness and strength of hydrogels [9,10]. In the last two decades, new approaches have been used to improve toughness: interpenetrating network hydrogels [11], double-network (DN) hydrogels [12,13], nanocomposite hydrogels [14,15], slide-ring hydrogels [16], and others [17–19]. DN hydrogels have high mechanical performance, which can be adjusted by modulating the inter and/or intramolecular interactions and within or between two network structures, by different crosslinkers

and/or crosslinking methods [20]. DN hydrogels have two interpenetrating networks with contrasting physical structures and properties: a rigid and brittle first network that breaks easily under large deformation to dissipate energy, while the soft and ductile second network contributes to stretchability and allows to return to the original configuration after deformation [21]. Nevertheless, the rupture of the covalent DN hydrogels network leads to permanent and irreversible damage, making recovery after initial loading difficult and leading to failure of the material under repeated loading [22]. The introduction of reversible, sacrificial, noncovalent bonds into the first network overcomes this limitation, which is due to the disruption–recrosslinking behaviour of physical networks [23,24]. The hybrid, physically and chemically crosslinked DN hydrogels have improved self-recovery capacity and fatigue resistance, which is extremely important in, for example, iterative soft load-bearing tissues, actuators, and implantable devices [25–27].

The best physical network for hybrid DN hydrogels are ionically crosslinked networks, composed of polysaccharides and multivalent ions [28]. Suo *et al.* [12] demonstrated that simultaneously ionically

---

* Corresponding author.
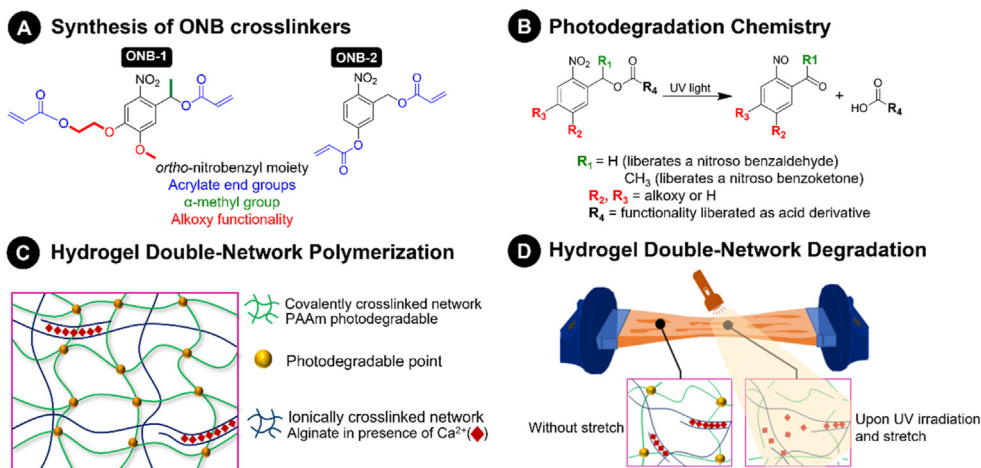 *E-mail address:* jcoelho@eq.uc.pt (J.F.J. Coelho).

Fig. 1. Overview of the approach: A) Synthesis of two o-nitrobenzyl (ONB) crosslinkers with different labile bonds. B) Photocleavage of ONB crosslinkers upon UV irradiation, forming an aromatic nitroso compound and a carboxylic acid. The R1 group determines the rate of photodegradation and the nature of resulting cleavage products. C) Structure of the alginate/PAAm hydrogels. In a polyacrylamide hydrogel, the polymer chains form covalent crosslinks through prepared ONB crosslinkers. The alginate hydrogel is formed by the ionic crosslinks through Ca^{2+} and. the G-blocks. D) After UV irradiation of the DN hydrogel, the ONB crosslinkers undergo an irreversible photocleavage, breaking the polyacrylamide hydrogel crosslinks. When stretched the PAAm network cannot stabilize the deformation, while the alginate network unzips progressively, resulting in a high loss of the material toughness.

Table 1
Different formulations used to prepare the DN hybrid hydrogels.

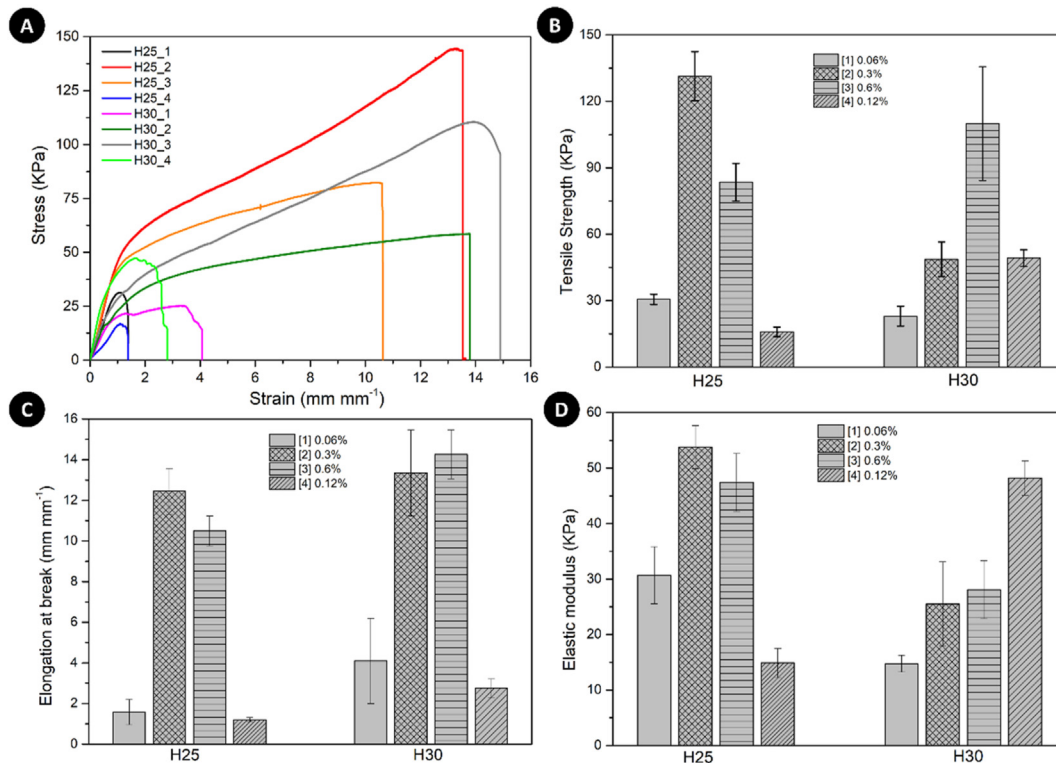| Type of hydrogel	AAm (wt%)	Na-Alg (wt %)	Crosslinker (%) (m crosslinker/m AAm)	APS (wt%)	TEMED (%) (m TEMED/m AAm)	$CaSO_4$ (%) (m $CaSO_4$/m AAm)	Solvent content (wt%)
Control	12.25	1.75	0.06	0.043	0.25	13.28	84 (water)
Photodegradable (H25 and H30)	12.25	1.75	0.06 0.3 0.6 0.12	0.043	0.25	13.28	86 (water + DMSO)

Fig. 2. Mechanical properties of photodegradable DN hydrogels determined by tensile tests: A) Stress-strain curves of gels with different percentages of DMSO (25–30 vol%) and amounts of covalent photodegradable crosslinker, ONB-1 (0.06%, 0.3%, 0.6% and 0.12% of ONB-1 is represented by 1, 2, 3 and 4, respectively). Each test was performed by pulling the samples at a constant rate of 20 mm min^{-1}. B) Tensile strength; C) Elongation at break; D) Elastic modulus calculated from the initial slopes of the stress-strain curves. The error associated with the values presented is the standard deviation of the five valid tests.
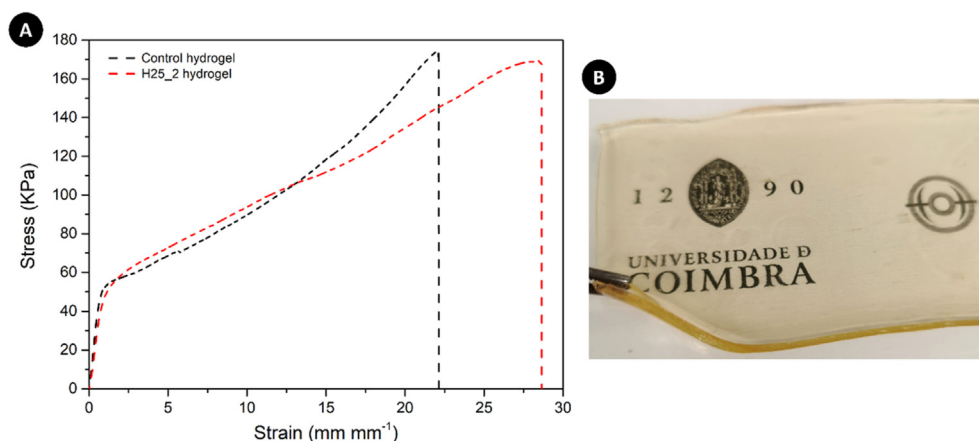
Fig. 3. Mechanical properties of DN hydrogels determined by tensile tests: A) Stress-strain curves of the control hydrogel and the photodegradable hydrogel (H25_2). Each test was performed by pulling the samples at a constant rate of 100 mm·min^{-1} until rupture; B) Photodegradable hydrogel.

Table 2

Mechanical properties of DN hydrogels: tensile strength, elongation at break, elastic modulus, and fracture energy. The error associated with the presented values is the standard deviation of the five valid tests.

Mechanical properties	Hydrogel samples	
	Control	H25_2
Tensile strength (kPa)	165.4 ± 7.5	165.7 ± 15.7
Elongation at break (mm mm^{-1})	23.5 ± 2.2	27.9 ± 3.9
Elastic modulus (kPa)	53.4 ± 5.9	56.2 ± 3.5
Fracture energy (J m^{-2})	6026.2 ± 649	6604.4 ± 557

(alginate) and covalently (acrylamide, AAm) crosslinked networks form a notch-insensitive hybrid hydrogel that could be stretched over 20-fold of its original shape with fracture energy of 9000 J m^{-2}. Although rapid and promising progress has been made in the synthesis of mechanically robust hydrogels, a major problem remains unsolved. The properties of these hydrogels are usually fixed at the time of preparation, making it impossible to subsequently tune them afterward, [29]. Also, most of the polymers used to form the crosslinked network are not biodegradable [30] (e.g., PAAm). Biodegradable hydrogel networks based on cellulose, chitosan, and alginate have been investigated by several groups [31–33], but these networks are inadequate in terms of mechanical and chemical

resilience. The synthesis of highly stretchable and tough hydrogels that can degrade in response to an external stimulus remains a challenge. The incorporation of stimuli-responsive units into the hydrogels would allow their properties to be changed in response to an externally applied stimulus [34]. Light has the advantage of allowing precise spatial and temporal control by using lights with different wavelengths, intensities, and irradiation times [35,36]. The most used photolabile core used in polymers are *o*-nitrobenzyl (ONB) derivatives [37]. Its mechanism of photolysis by UV light is well known, and they are considered biocompatible [38]. Chemical modifications of the aromatic ring or benzyl position of ONB derivatives [39,40], resulted in a redshift of the absorption window, improved cytocompatibility, increased rate of photocleavage, and the prevention of the formation of toxic by-products after photolysis [41]. Therefore, structural tuning of the chemical structure of ONB linkers offers the possibility of developing materials with light-tuneable mechanical properties [38,42]. In this work, photocleavable highly stretchable and tough DN hydrogels are prepared for the first time. Networks disruption can be remotely triggered using cytocompatible light wavelength. Alginate/PAAm DN hydrogels are prepared by a one-step method. Divalent cations (Ca^{2+}) were used for ionic crosslinking of alginate, while PAAm was covalently crosslinked by a new ONB-based bifunctional crosslinker. Since the new ONB-crosslinker is not water-soluble, a special protocol was developed using an optimized ratio of between DMSO/water to enable the preparation of the hydrogels.
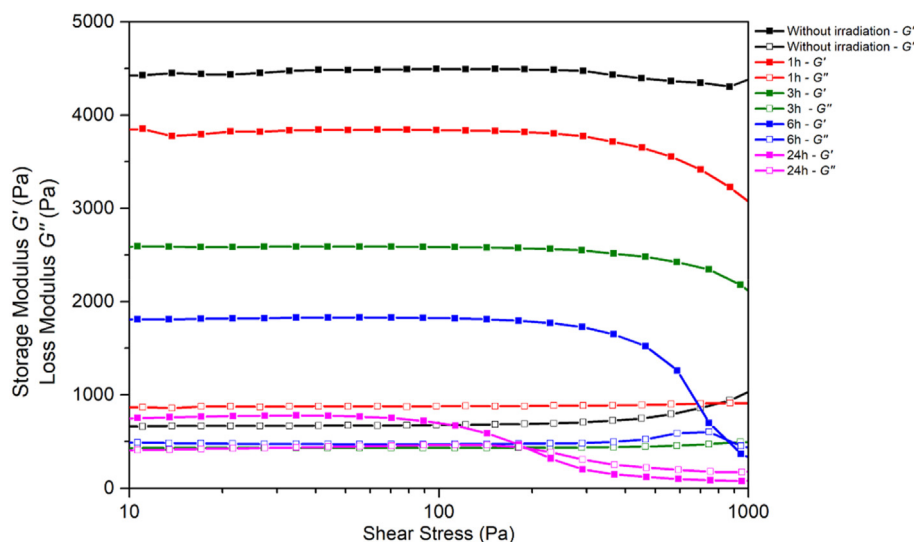

Fig. 4. Rheological analyses of photodegradable hydrogels (H25_2) before and after UV irradiation, at different irradiation times.
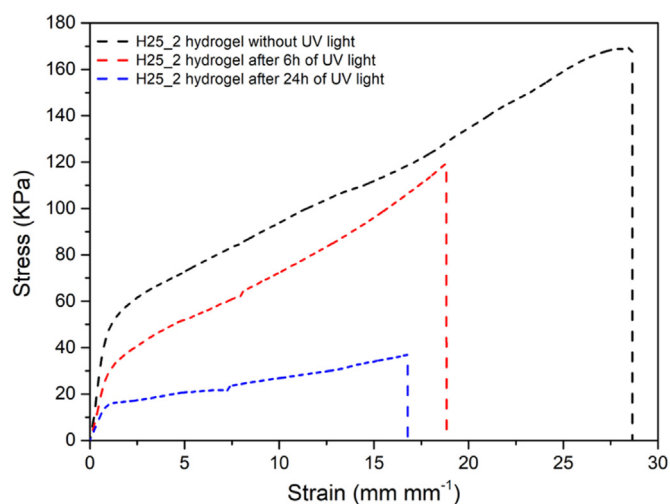
Fig. 5. Stress-strain curves of photodegradable hydrogel (H25_2) without irradiation and after 6 and 24 h of UV irradiation. Each test was performed by pulling the samples to rupture at a constant velocity of 100 mm min^{-1}.

Table 3
Mechanical properties of DN hydrogels after UV irradiation: tensile strength, elongation at break and elastic modulus. The error associated with the presented values is the standard deviation of the five valid tests.

Mechanical properties	Hydrogel samples	
	H25_2 (6 h)	H25_2 (24 h)
Tensile strength (kPa)	118.46 ± 8.8	32.8 ± 4.4
Elongation at break (mm mm^{-1})	18.9 ± 6.2	18.5 ± 3.8
Elastic modulus (kPa)	33.4 ± 7.5	15.2 ± 4.8

Hydrogels were characterized in terms of their mechanical and photodegradability as well as their in vitro toxicity. It is envisioned that these photodegradable hydrogels, with their improved properties, will open up new applications in various fields including artificial tissues, bio-electronics, and flexible sensors. As an example, we showed the application of these hydrogels in bio-potential acquisition for wearable electrocardiography and compared their skin-electrode impedance with the commonly used medical grade Ag/AgCl electrodes.

2. Results and discussion

The aim of this work is to develop highly stretchable and tough hydrogels that can be degraded when needed, by irradiation of ONB moieties inside the two polymer networks (Fig. 1).

2.1. Photodegradable properties of the crosslinkers

The photodegradation of ONB is triggered by the reduction of the NO$_2$ group to the nitroso group and the insertion of an oxygen atom into the C–H bond at the benzylic position [43–45]. Consequently, irradiation with 260 nm light leads to the release of carboxylic acid and o-nitrosobenzaldehyde (or nitrosoketone) as by-products [46]. Structural changes of ONB affect the molar absorptivity (ε), yield and kinetics of the photocleavage reaction [38]. The introduction of an α-CH$_3$ group at the benzylic carbon atom speeds up the cleavage and release a ketone by-product instead of an aldehyde [47]. Also, one or more alkoxy groups in *meta* and *para* positions cause a redshift in the absorption spectrum and increase the rate of photocleavage [40]. The balance between the strong electron-withdrawing capacity of the NO$_2$ group and the
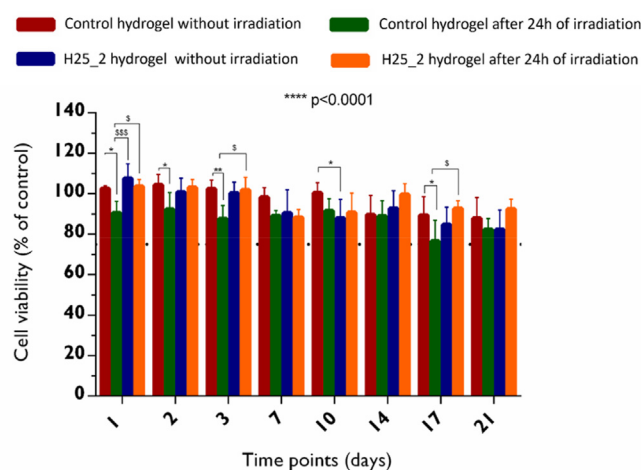

Fig. 7. Results of in vitro cell viability when cells are exposed to gel conditioned medium. Data are represented as means ± standard deviation of three independent experiments with n = 3 samples for each treatment. The statistical significance was indicated as ****p < 0.0001 by two-way ANOVA with a Tukey post-hoc test.
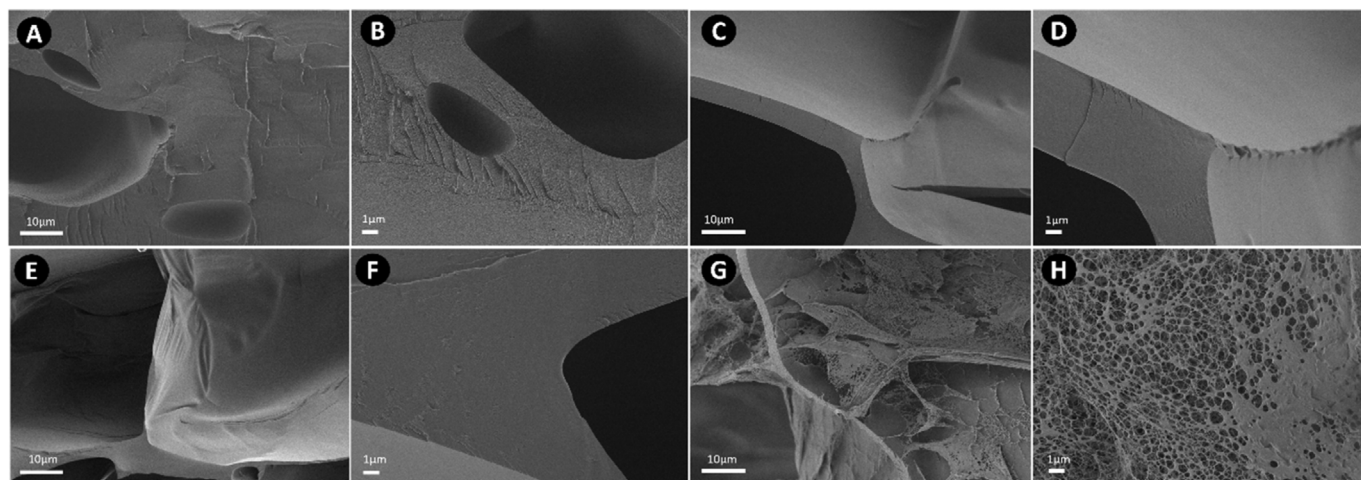

Fig. 6. Representative SEM images of the cross-section morphologies of control hydrogels before (A and B) and after 24 h of irradiation (C and D), and photodegradable hydrogels before (E and F) and after 24 h of irradiation (G and H).
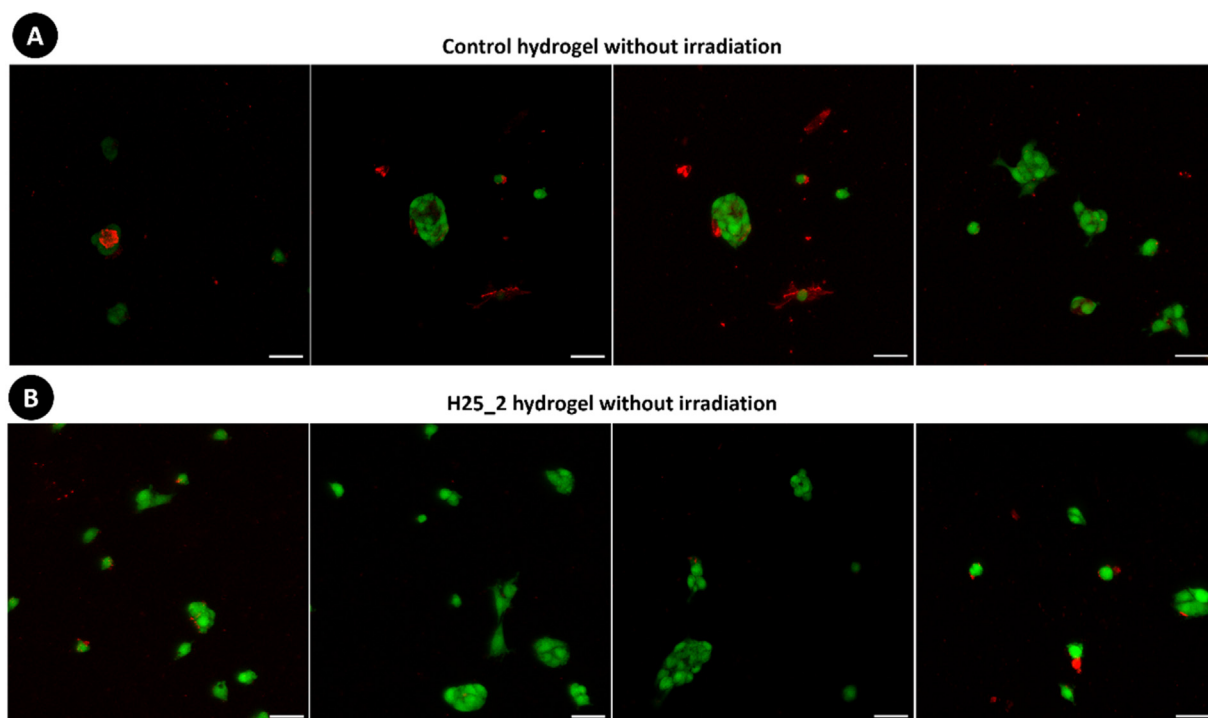
Fig. 8. Representative Z-stack images captured by confocal microscopy that were reconstructed into a 3D image using ZEN 2.3 Imaging Software. Green cells indicate live cell colonizing the surface and interior of the hydrogels, while dead cells appear in red colour, after 48 h of incubation. The white bar shown the scale is 100 pixel.

electron-donating effect of the OCH_3 group in *para* position to the NO_2 allows a shorter irradiation time for the cleavage of the photolabile compound [48]. The synthesis of the new photodegradable ONB crosslinkers exploits both the α-CH$_3$ group at the benzylic carbon and the alkoxy functionality (ONB-1, Fig. 1A and Figure S1). These groups promote efficient photocleavage [29], making ONB-1 an excellent candidate for weakening the polymeric network upon irradiation. For comparison, an ONB crosslinker without both substituents was also synthesized (ONB-2, Fig. 1A and Figure S1).

The spectroscopical properties of the two synthesized crosslinkers were studied by UV-VIS spectrophotometry and ^{1}H NMR. The absorption spectra of ONB-1 showed three maximum absorption peaks at 243, 301 and 335 nm, while ONB-2 exhibited only one maximum absorption peak at 273 nm (Figure S10). This change in the absorption profile between the two ONB crosslinkers suggests that the presence of the alkoxy group leads to a redshift in the spectrum [40,49]. Small structural changes in the ONB crosslinker lead to significant changes in ε, because at a given wavelength ε affects the photodegradation rate, and very low values of ε, imply limited or no photodegradation [50]. As observed for the ONB-1, the calculated ε_{243} is 13892 M^{-1}cm^{-1}, ε_{301} is 6289 M^{-1}cm^{-1} and ε_{335} is 6122 M^{-1}cm^{-1}, while for the ONB-2 crosslinker the calculated ε_{243} is 4090 M^{-1}cm^{-1}, ε_{301} is 4050 M^{-1}cm^{-1} and ε_{335} is 946 M^{-1}cm^{-1} (Table S1, Figure S11-Figure S18). ε decreases with increasing wavelength, consistent with previous reports [50,51]. The red shift in absorption causes photolysis at a higher wavelength that also minimizes potential tissue damage and improves cytocompatibility [52]. Rapid photocleavage kinetics and a high ε result in a faster-degrading crosslinker, which shortens the irradiation time [50]. ONB-1 and 2 were analysed by ^{1}H NMR before and after irradiation with UV light in CHCl$_3$. Photodegradation of ONB-1 yields a ketone and a carboxylic acid (Fig. 1B). ^{1}H NMR spectrum of ONB-1 (Figure S19) shows the appearance of a new signal (m) at 2.5 ppm, belonging to the protons of the ketone –CH$_3$ group, indicating the cleavage of the ONB core. After 1 h of irradiation, the photocleavage conversion was 57%, and after 6 h was 100%. The ^{1}H NMR spectrum of ONB-2 (Figure S20), shows the appearance of a new signal (i) at 10.45 ppm, corresponding to the proton of the aldehyde

group of *o*-nitrosobenzaldehyde. However, after 1, 3 and 6 h, the photodegradation was only 3, 6, and 10%, respectively. To increase the photodegradation, the irradiation was extended to 24 h, but the conversion levelled off to 10%. This could be due to the release of *o*-nitrosobenzaldehyde, which can act as an internal light filter [44,49,53]. The compound ONB-1 exhibits faster photodegradation kinetics, due to the presence of an α-CH$_3$ group on the benzylic carbon, so it was selected as crosslinker for hydrogel preparation.

2.2. Preparation of the photodegradable DN hybrid hydrogels

The photodegradable DN hybrid hydrogels were prepared using an ionically crosslinked Ca^{2+} alginate network, and a covalently crosslinked PAAm network. In an aqueous solution, gelation of alginate occurs when divalent cations (such as Ca^{2+}) ionically interact with α-L-guluronic acid blocks (G-blocks) from different alginate chains, to form the first network [54]. The PAAm network, in turn, was prepared by conventional free radical polymerization of AAm in the presence of the photodegradable crosslinker. Normally, hydrogels are prepared using water as solvent because reagents are water soluble. However, as ONB-1 is hydrophobic, DMSO is added as co-solvent to promote its dissolution. Although DMSO dissolves ONB-1, it also causes rapid gelation of aqueous alginate solutions [55]. Therefore, the water/DMSO ratio must be carefully optimized to ensure that ONB-1 is completely dissolved, but without causing premature gelation of the Na-Alg solution. To this end, various amounts of DMSO were added to Na-Alg solutions (Table S2). Visual inspection showed that the solution still flowed when 25 vol% and 30 vol% DMSO was added (Figure S21). In contrast, solutions with more than 40 vol% DMSO gelled. Furthermore, a PAAm network must form under these conditions. The PAAm networks were considered finish if no gravitational flow occurred when the glass flash was inverted. With a curing time of 24 h, the lowest amount of DMSO to obtain a gel was 25 vol% (Table S3, Figure S22). Thus, photodegradable hydrogels (labelled as H25 and H30) were developed with 25 vol% and 30 vol% DMSO, respectively. Different concentrations of ONB-1 crosslinker allowed the investigation of the response of the hydrogel to the crosslink density
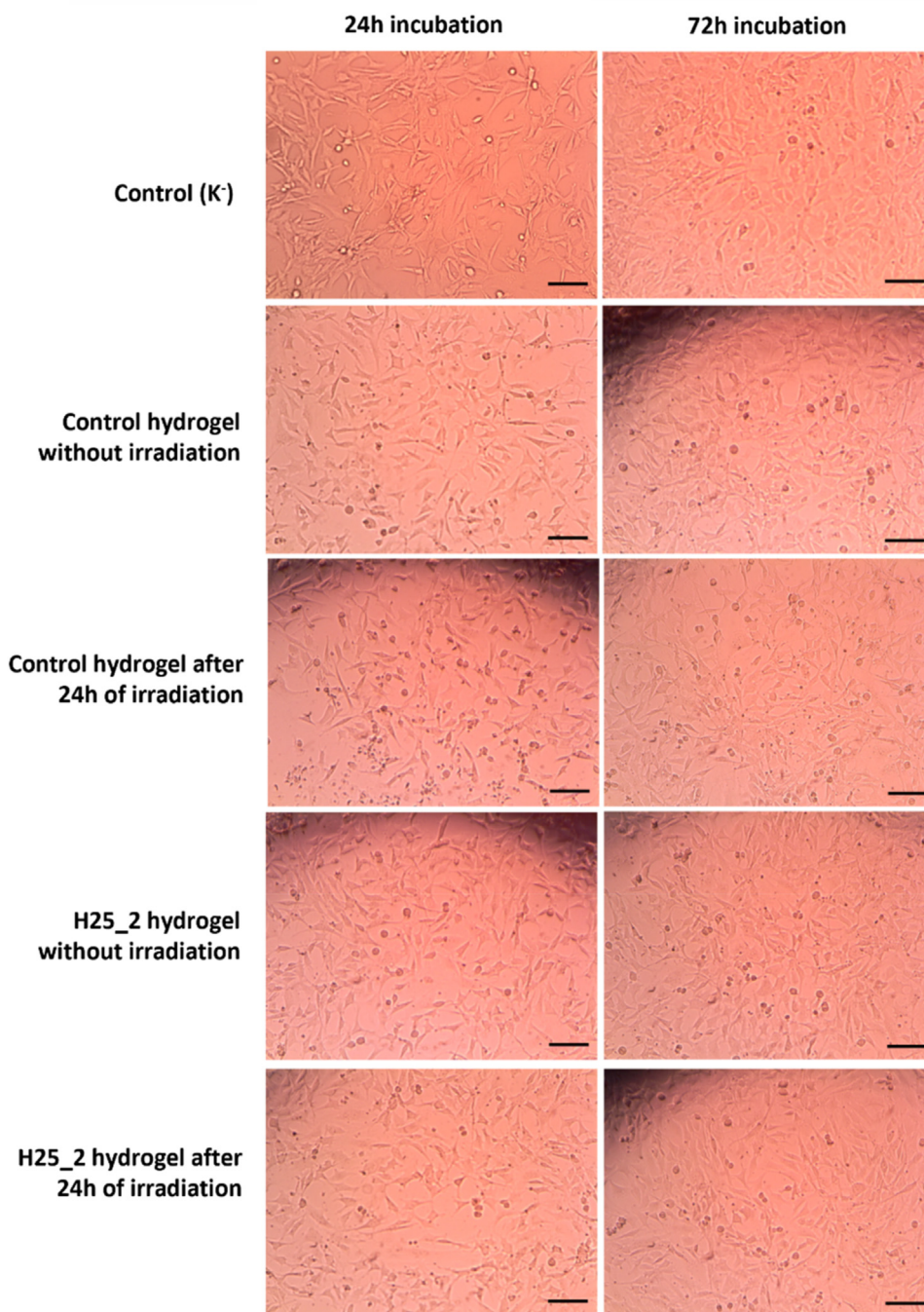
Fig. 9. Microscopic phase contrast images of NIH3T3 cells grown on the surface of the hydrogels at different degradation time intervals - after 24 h incubation (top) and 72 h incubation (bottom). The magnification of all the photographs is the same with the scale bar equals to 200 μm.

(Table S4). The concentrations of APS, TEMED and CaSO$_4$ were used according to previous work and kept constant in all formulations [12]. The control hydrogel was prepared without DMSO, and with MBAA instead of the ONB-1 crosslinker to compare the mechanical properties [12]. The amounts of each compound to prepare the control and photodegradable hydrogels are shown in Table 1. After the curing step, the average solvent content of the control and photodegradable hydrogels was 84% and 86%, respectively (Figure S23).

2.3. Mechanical properties of the photodegradable DN hybrid hydrogels

The effect of the amounts of DMSO and ONB-1 crosslinker on the mechanical properties of the photodegradable DN hybrid hydrogels was investigated. Tensile tests were performed by pulling the samples to rupture at a constant strain rate of 20 mm min^{-1} (Fig. 2). This strain rate was chosen because some samples exhibited minor brittleness and were difficult to test at higher strain rates.

Intermediate concentrations of ONB-1 (0.3% and 0.6%) give the hydrogels with the best properties (higher tensile strength, higher elongation at break and higher elastic modulus). For the H25 and H30, 0.3% and 0.6% were the best concentrations, respectively. Hydrogels containing only 0.06% ONB-1 exhibited poor mechanical properties. A low ONB-1 concentration results in a loosely crosslinked network, that cannot withstand mechanical stress. On the other hand, hydrogels with the
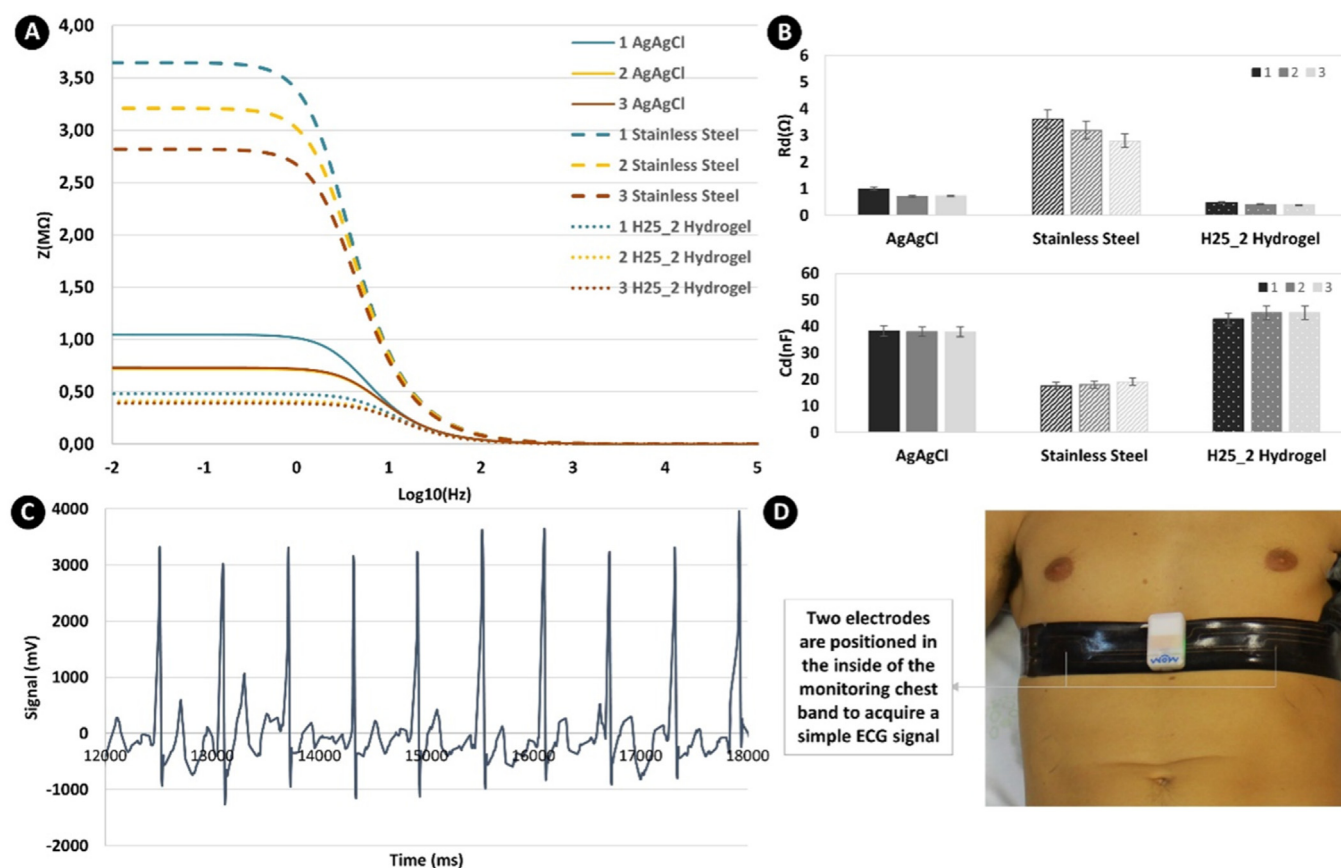
Fig. 10. Case study of application in bioelectronics: A) Skin-electrode impedance in function of the frequency, for three different electrodes: Ag/AgCl, stainless steel and hydrogel electrodes. B) Cd and Rd values for all electrodes after fitting to the electrical equivalent circuit, during the impedance analysis. C) Portion of the ECG signal obtained with the hydrogel electrodes. D) Setup used for the acquisition of the ECG signal: monitorization chest band with integrated hydrogel electrodes.

highest ONB-1 concentrations were also mechanically poor. Denser crosslinked networks, imply PAAm chains with a shorter length. When a load is applied and the chain breaks, the energy stored in the entire chain is dissipated, resulting in low fracture energy [12]. Formulations containing 25 vol% DMSO exhibit a more uniform change in mechanical properties when the amount of ONB-1 is changed. This suggests that increasing the amount of DMSO could affect the polymerization and crosslinking steps, resulting in hydrogels with greater variability in properties. These results indicate that the best formulation contains 25 vol% DMSO and 0.3% ONB-1 (H25_2), and it was selected for further testing. The effect of strain rate on the mechanical properties of the hydrogels was investigated. Tensile tests were performed at three different strain rates: 20, 50, and 100 mm·min^{-1} (Figure S24). The strain-softening behaviour of the stress-strain curves is typical of tough hydrogels, which can be attributed to the breaking of the sacrificial bonds [56]. As expected, the elastic modulus increases with increasing strain rate, while the stretchability decreases. At strain rates of 50 and 100 mm min^{-1}, the values for elastic modulus are similar (Table S5). To measure dehydration during the tensile test, all specimens were weighed before and after the tests. It was found that the hydrogels lost only ~3% of the original weight at a higher stretching rate (Figure S25). To minimize the change in properties due to water evaporation [57], a strain rate of 100 mm min^{-1} was used in the subsequent tensile tests, where the properties of the control hydrogel and the light-responsive hydrogel (H25_2) were compared.

The stress-strain curves of the control and light-responsive hydrogels showed a similar mechanical behaviour (Fig. 3) and their properties are in accordance with the previous work [12]. The tensile strength, elongation at break and elastic modulus were 165.4 ± 7.5, 23.5 ± 2.2, and 53.4 ± 5.9 kPa for the control hydrogel, and 165.7 ± 18.7, 27.9 ± 3.9,

and 56.2 ± 3.5 kPa for the photodegradable gel, respectively (Table 2). The two hydrogels have similar fracture energies (Table 2, Figure S26). These results show that the replacement of MBAA by the photodegradable crosslinker, and the use of DMSO in the formulation, do not affect the mechanical properties. In fact, slightly better mechanical properties were obtained for the photodegradable hydrogel. These properties result from the synergistic effect achieved by the combination of a highly extensible network and another, less stretchable network, interpenetrated in a topological entanglement [58]. As a crack in the hydrogel progresses, the more stretchable network bridges the crack and transmits forces to the bulk of the hydrogel, while the less stretchable network ruptures over a significant volume of the hydrogel [59]. In this case, the PAAm network remains intact and acts as an entropic spring. In contrast, the alginate network serves as a toughener and gradually unzips, resulting in dissipation of stored energy and preventing catastrophic crack propagation in the bulk [60].

2.4. Photodegradation of the DN hybrid hydrogels

To understand the response of the photodegradable hydrogels, they were characterized by rheological and mechanical tests, and their morphology was evaluated by SEM before and after photoirradiation. Photodegradation was studied using the oscillatory amplitude sweep test to determine the changes in viscoelastic properties. The storage modulus (G′) and loss modulus (G″) were measured by the applied shear stress (Fig. 4). The photodegradable hydrogel without light exposure showed a linear range and the values of G′ and G″ remained unchanged over the entire range of shear stress. The G′ values were higher than the corresponding G″ values, indicating the elastic behaviour of the hydrogel [61]. Upon irradiation, both G′ and G″ values decreased, indicating softening

of the material. After 6 and 24 h of irradiation, the G′ curve intersected the G″ curve at a shear stress of 747 and 181 Pa, respectively. G′ was lower than G″ when the stress was above these critical values, indicating that the hydrogels changed from a solid to a liquid state, due to the breakdown of the network [62,63]. The photodegradation of the ONB-1 crosslinker caused the failure of the PAAm network. When the irradiated hydrogels are subjected to higher load stress, the photodegraded PAAm network cannot withstand the stress to its former extent, resulting in a severe loss of toughness of the material.

The photodegraded hydrogels were also evaluated by tensile tests (Fig. 5). Considering the rheological results, they were irradiated for 6 and 24 h. An increase in the irradiation time resulted in a greater decrease in the mechanical properties (Fig. 5), which can be attributed to the increasing destruction of crosslinker ONB-1 and the failure of the PAAm network. As expected, the elastic modulus [64], drastically decrease by 41% and 73% for samples irradiated for 6 and 24 h, respectively (Table 3) [64]. The tensile strength and elongation at break were 118.4 kPa and 18.9 for 6 h of UV light, and 32.8 kPa and 18.5 for 24 h of UV light, respectively (Table 3). With increasing irradiation time, more ONB-1 cores are photocleaved, leading to a further decrease of tensile strength, elastic modulus and tensile strain. Even though the hybrid hydrogel is composed of an interpenetrating network, the physically crosslinked network cannot respond efficiently to mechanical solicitations if the covalent network is irreversibly destroyed. The results obtained in the tensile tests are consistent with those obtained in the rheological tests.

SEM analysis was performed to observe the morphology of the cross-section before and after photodegradation (Fig. 6, Figure S27-S28). The morphology of the control hydrogel was also observed. Before irradiation, all hydrogels exhibited a homogeneous structure with a porous interpenetrating network, similar to other reports [65]. This morphology and interconnectivity between pores are beneficial for biomedical applications, as they facilitate cell adhesion/proliferation, and also drug delivery [66]. All hydrogels were irradiated for 24 h, as the greatest loss of properties occurred after this time, as indicated by the rheological and tensile tests. While the control hydrogels maintained their homogeneous porous structure regardless of irradiation (Fig. 6A–D), the photodegradable ones exhibited a porous structure interconnected with numerous circular holes after light exposure (Fig. 6G–H). One hypothesis, these pores are due to the migration of the soluble PAAm segments formed by the degradation of the PAAm network (Fig. 6E–H). This morphology analysis confirms the rheological and tensile tests. Since the hydrogel exhibits a higher porosity, after 24 h of irradiation, poor mechanical behaviour is expected. A photo of the photodegradable hydrogel before and after 24 h of irradiation is shown in Figure S29.

2.5. Cytocompatibility of the hydrogels

The potential cytotoxic effects of their degradation products were quantified using an AlamarBlue™ HS Cell Viability assay (indirect method). NIH3T3 fibroblast cells were exposed to gel-conditioned media (hydrogels with a thickness of 2 mm and a diameter of 8 mm diameter in 25 mL medium) at various time points (1–21 days of incubation), i.e., the cells were exposed to media in which the gels could continuously release soluble degradation products. The control and the light-responsive hydrogels (H25_2) without and after 24 h of irradiation were evaluated. Fig. 7 shows the relative cell viability (%) for NIH3T3 cells incubated with the extracts.

According to ISO 10993–5:1999, samples with cell viability greater than 75% can be considered non-cytotoxic. The viability of NIH3T3 cells exposed to the gel-conditioned medium was always >75%, indicating that any degradation by-products that may have been generated did not affect cell viability for 21 days. Compared with control hydrogels, the viability of cells exposed to the conditioned medium with photodegradable hydrogel after photodegradation (H25_2) was slightly higher and statistically significant at 1, 3 and 17 days.

To corroborate these observations, we also evaluated the interaction of non-irradiated hydrogels (control hydrogel and H25_2 hydrogel) with NIH3T3 cells by confocal microscopy. For this purpose, NIH3T3 cells seeded on the surface of hydrogels were stained with Calcein-AM and BOBO-3 Iodide (LIVE/DEAD™ Cell Imaging Kit, Invitrogen) to compare cell viability in both hydrogels. BOBO-3 Iodide (dead cell indicator) was used to detect apoptotic and necrotic cells and Calcein-AM, a cell permeant dye, as an indicator of live cells. Viable cells emit light green fluorescence and non-viable cells emit red fluorescence. Fluorescence images of NIH3T3 cells cultured with control hydrogel and H25_2 hydrogel are shown in Fig. 8A and 8B, respectively. Z-stack images showed that the cells internalized the hydrogels after 48 h. Cells in the control hydrogel grew poorly and some of the cells showed irregular morphology, a significant number of dead cells was detected (Fig. 8A). In the H25_5 hydrogel, the number of cells growing inside the hydrogel was higher, its morphology was good and no large number of dead cells was observed (Fig. 8B). These observations were consistent with the results of the AlamarBlue™ HS Cell Viability assay and with previous reports [67, 68] in which the control hydrogels showed a decrease in cell viability, suggesting that the MBAA crosslinker has some effect on cells. This study highlights the good cytocompatibility and safety of the developed ONB-1 based hydrogels and the minimal acute cytotoxicity over long periods of time, which is important for any biomedical application.

2.6. Cell growth and morphology analysis

To evaluate the interaction between the cells and the developed hydrogels, NIH3T3 cells were cultured on the hydrogel surface. After 1 day of culture, only a few NIH3T3 cells were attached, but the cells spread very well on the surface of the hydrogels; and showed a round-shaped configuration with some cytoplasmic extensions (cell elongation) (Fig. 9A–D). As shown in Fig. 9 D-G, the NIH3T3 cells proliferated significantly on the surface of the hydrogels after the third day of sowing and remained viable in contact with the hydrogel and negative control (K⁻). Moreover, the cells are distributed over a large area, have the typical fibroblastic morphology, and a continuous cell layer has formed [69]. After 72 h of incubation, the photodegradable hydrogels were completely destroyed by irradiation, but their degradation products allow cell proliferation to a large extent. Thus, with or without irradiation, the photodegraded hydrogels (H25_2) exhibit good cell adhesion and excellent cytocompatibility.

2.7. Case study of application in bioelectronics

An emerging application of hydrogels is in wearable biomonitoring [70–72]. Conductive hydrogel electrodes can be used to measure biopotentials, for monitoring of muscles, heart, and brain activity by electrocardiography (ECG), electromyography (EMG), and electroencephalography (EEG) [70]. To assess their suitability, we evaluated the quality of the interface between the skin and the electrodes through impedance spectroscopy in a range of 10^{-2} Hz–10^5 Hz. Tests were performed for 9 pairs of electrodes 3 hydrogels pairs, 3 stainless steel 316 L, and 3 Medical grade Ag/AgCl pairs (see SI for more information). Fig. 10A, shows the fitting to the equivalent skin-electrode impedance fitting. Our hydrogel electrodes exhibit a lower impedance even when compared to medical grade Ag/AgCl electrodes, especially at the low frequencies, which are the frequencies of interest for bioelectronics applications such as EMG, ECG, and EEG. Fig. 10B, shows the R_d and C_d values. The hydrogel electrodes offer the highest C_d values and the lowest R_d values, which are both desired properties. Two hydrogels were integrated into a monitoring chest band (Fig. 10D), to acquire ECG signal. As can be seen in Fig. 10C, an excellent signal amplitude can be observed along with an easy visualization of the QRST complex.

As the interest in disposable wearable bioelectronics is rapidly growing, the use of degradable materials is a very important consideration for a sustainable future. This can be extended to other growing

applications of hydrogels in energy storage batteries and Supercapacitors.

3. Conclusion

New photodegradable ONB crosslinkers were synthesized and incorporated into alginate/PAAm DN hydrogels, to develop for the first time highly stretchable and tough hydrogel, with triggerable photodegradation. The hydrogels were characterized by mechanical, photodegradation and cytocompatibility tests. Replacing MBAA with ONB crosslinkers, and despite the use of DMSO, excellent mechanical performances are retained. Rheological and mechanical analysis demonstrated the loss of properties of ONB-1 based DN hydrogel after irradiation, confirming the efficient destruction of the covalently crosslinked network, resulting in the loss of mechanical properties. SEM analyses also visually confirmed the network photodegradation. Cell viability and proliferation assays confirmed that these hydrogels and their photodegradation products do not induce any cytotoxicity on the NIH3T3 cell line.

It is envisaged that the design of innovative on-demand photodegradable hydrogels which are tough, and safe provides an interesting alternative to a wide range of biomedical applications such as wearable devices, bioelectronics interfaces, and mechanically resilient batteries and supercapacitors.

Data availability

All data needed to evaluate the conclusions in the paper are present in the paper and/or the Supplementary Information. Additional data related to this paper may be requested from the authors.

Credit author statement

Rita G. Fonseca: Conceptualization, Methodology, Investigation, Visualization, Writing – original draft. **Francesco De Bon**: Conceptualization, Writing – review & editing. **Patrícia Pereira**: Investigation, Formal analysis, Writing – original draft. **Marta Freitas:** Investigation. **Francisca M. Carvalho:** Investigation, Writing – original draft. **Mahmoud Tavakoli**: Methodology, Writing – review & editing. **Arménio C. Serra**: Resources, Writing – review & editing, Supervision, Project administration. **Ana C. Fonseca**: Validation, Resources, Writing – review & editing. **Jorge F. J. Coelho**: Conceptualization, Methodology, Writing – review & editing, Supervision, Project administration.

Declaration of competing interest

The authors declare that they have no known competing financial interests or personal relationships that could have appeared to influence the work reported in this paper.

Acknowledgements

Appendix A. Supplementary data

Supplementary data to this article can be found online at https:// doi.org/10.1016/j.mtbio.2022.100325.

References

[1] Q. Chai, Y. Jiao, X. Yu, Hydrogels for biomedical applications : their characteristics and the mechanisms behind them, Gels 3 (2017) 1–15, https://doi.org/10.3390/gels3010006.

[2] X. Zhou, B. Guo, L. Zhang, G.-H. Hu, Progress in bio-inspired sacrificial bonds in artificial polymeric materials, Chem. Soc. Rev. 46 (2017) 6301–6329, https://doi.org/10.1039/c7cs00276a.

[3] P. Matricardi, C. Di Meo, T. Coviello, W.E. Hennink, F. Alhaique, Interpenetrating Polymer Networks polysaccharide hydrogels for drug delivery and tissue engineering, Adv. Drug Deliv. Rev. (2013) 1–16, https://doi.org/10.1016/j.addr.2013.04.002.

[4] A. Vashist, A. Vashist, Y.K. Gupta, S. Ahmad, Recent advances in hydrogel based drug delivery systems for the human body, J. Mater. Chem. B (2014) 147–166, https://doi.org/10.1039/c3tb21016b.

[5] L. Li, Y. Shi, L. Pan, Y. Shi, G. Yu, Rational design and applications of conducting polymer hydrogels as electrochemical biosensors, J. Mater. Chem. B. 3 (2015) 2920–2930, https://doi.org/10.1039/c5tb00090d.

[6] P.A. Lopes, D. Vaz Gomes, D. Green Marques, P. Faia, J. Góis, T.F. Patrício, J. Coelho, A. Serra, A.T. de Almeida, C. Majidi, M. Tavakoli, Soft bioelectronic stickers: selection and evaluation of skin-interfacing electrodes, Adv. Healthc. Mater. 8 (2019) 1–11, https://doi.org/10.1002/adhm.201900234.

[7] C. Leal, P.A. Lopes, A. Serra, J.F.J. Coelho, A.T. De Almeida, M. Tavakoli, Untethered disposable health monitoring electronic patches with an integrated Ag2O-Zn battery, a AgInGa current collector, and hydrogel electrodes, ACS Appl. Mater. Interfaces 12 (2020) 3407–3414, https://doi.org/10.1021/acsami.9b18462.

[8] X. Cao, C. Jiang, N. Sun, D. Tan, Q. Li, S. Bi, J. Song, Recent progress in multifunctional hydrogel-based supercapacitors, J. Sci. Adv. Mater. Devices. 6 (2021) 338–350, https://doi.org/10.1016/j.jsamd.2021.06.002.

[9] F. Oveissi, D.F. Fletcher, F. Dehghani, S. Naficy, Tough hydrogels for soft artificial muscles, Mater. Des. 203 (2021), https://doi.org/10.1016/j.matdes.2021.109609.

[10] P. Dorishetty, N.K. Dutta, N.R. Choudhury, Bioprintable tough hydrogels for tissue engineering applications, Adv. Colloid Interface Sci. 281 (2020), 102163, https://doi.org/10.1016/j.cis.2020.102163.

[11] G. Du, L. Nie, G. Gao, Y. Sun, R. Hou, H. Zhang, T. Chen, J. Fu, Tough and biocompatible hydrogels based on in situ interpenetrating networks of dithiol-connected graphene oxide and poly(vinyl alcohol), ACS Appl. Mater. Interfaces 7 (2015) 3003–3008, https://doi.org/10.1021/acsami.5b00184.

[12] J. Sun, X. Zhao, W.R.K. Illeperuma, O. Chaudhuri, K.H. Oh, D.J. Mooney, J.J. Vlassak, Z. Suo, Highly stretchable and tough hydrogels, Nature 489 (2012) 133–136, https://doi.org/10.1038/nature11409.

[13] Q. Chen, D. Wei, H. Chen, L. Zhu, C. Jiao, G. Liu, L. Huang, J. Yang, L. Wang, J. Zheng, Simultaneous enhancement of stiffness and toughness in hybrid double-network hydrogels via the first, physically linked network, Macromolecules 48 (2015) 8003–8010, https://doi.org/10.1021/acs.macromol.5b01938.

[14] P. Lin, S. Ma, X. Wang, F. Zhou, Molecularly engineered dual-crosslinked hydrogel with ultrahigh mechanical strength, toughness, and good self-recovery, Adv. Mater. 27 (2015) 2054–2059, https://doi.org/10.1002/adma.201405022.

[15] C.W. Chang, A. Van Spreeuwel, C. Zhang, S. Varghese, PEG/clay nanocomposite hydrogel: a mechanically robust tissue engineering scaffold, Soft Matter 6 (2010) 5157–5164, https://doi.org/10.1039/c0sm00067a.

[16] C. Zhu, C. Ninh, C.J. Bettinger, Photoreconfigurable polymers for biomedical applications: chemistry and macromolecular engineering, Biomacromolecules 15 (2014) 3474–3494, https://doi.org/10.1021/bm500990z.

[17] G. Song, L. Zhang, C. He, D.C. Fang, P.G. Whitten, H. Wang, Facile fabrication of tough hydrogels physically cross-linked by strong cooperative hydrogen bonding, Macromolecules 46 (2013) 7423–7435, https://doi.org/10.1021/ma401053c.

[18] D.C. Tuncaboylu, M. Sari, W. Oppermann, O. Okay, Tough and self-healing hydrogels formed via hydrophobic interactions, Macromolecules 44 (2011) 4997–5005, https://doi.org/10.1021/ma200579v.

[19] A.M.S. Costa, J.F. Mano, Extremely strong and tough hydrogels as prospective candidates for tissue repair – a review, Eur. Polym. J. 72 (2015) 344–364, https://doi.org/10.1016/j.eurpolymj.2015.07.053.

[20] J. Wang, L. Lou, J. Qiu, Super-tough hydrogels using ionically crosslinked networks, J. Appl. Polym. Sci. 136 (2019) 1–9, https://doi.org/10.1002/app.48182.

[21] J.P. Gong, Why are double network hydrogels so tough? Soft Matter 6 (2010) 2583–2590, https://doi.org/10.1039/b924290b.

[22] M.H. Ghanian, H. Mirzadeh, H. Baharvand, In situ forming, cytocompatible, and self-recoverable tough hydrogels based on dual ionic and click cross-linked alginate, Biomacromolecules 19 (2018) 1646–1662, https://doi.org/10.1021/acs.biomac.8b00140.

[23] Q. Chen, L. Zhu, H. Chen, H. Yan, L. Huang, J. Yang, J. Zheng, A novel design strategy for fully physically linked double network hydrogels with tough, fatigue resistant, and self- Healing properties, Adv. Funct. Mater. 25 (2015) 1598–1607, https://doi.org/10.1002/adfm.201404357.

[24] H.J. Zhang, T.L. Sun, A.K. Zhang, Y. Ikura, T. Nakajima, T. Nonoyama, T. Kurokawa, O. Ito, H. Ishitobi, J.P. Gong, Tough physical double-network hydrogels based on amphiphilic triblock copolymers, Adv. Mater. 28 (2016) 4884–4890, https://doi.org/10.1002/adma.201600466.

[25] L. Li, K. Zhang, T. Wang, P. Wang, B. Xue, Y. Cao, L. Zhu, Q. Jiang, Biofabrication of a biomimetic supramolecular-polymer double network hydrogel for cartilage regeneration, Mater. Des. 189 (2020), 108492, https://doi.org/10.1016/j.matdes.2020.108492.

[26] N. Kitamura, M. Yokota, T. Kurokawa, J.P. Gong, K. Yasuda, In vivo cartilage regeneration induced by a double-network hydrogel: evaluation of a novel therapeutic strategy for femoral articular cartilage defects in a sheep model, J. Biomed. Mater. Res., Part A 104 (2016) 2159–2165, https://doi.org/10.1002/jbm.a.35745.

[27] S. Liu, L. Li, Ultrastretchable and self-healing double-network hydrogel for 3D printing and strain sensor, ACS Appl. Mater. Interfaces 9 (2017) 26429–26437, https://doi.org/10.1021/acsami.7b07445.

[28] Y. Yang, X. Wang, F. Yang, L. Wang, D. Wu, Highly elastic and ultratough hybrid ionic–covalent hydrogels with tunable structures and mechanics, Adv. Mater. 30 (2018) 1–9, https://doi.org/10.1002/adma.201707071.

[29] F. Ercole, H. Thissen, K. Tsang, R.A. Evans, J.S. Forsythe, Photodegradable hydrogels made via RAFT, Macromolecules 45 (2012) 8387–8400, https://doi.org/10.1021/ma301315q.

[30] L.H. Christensen, V.B. Breiting, A. Aasted, A. Jørgensen, I. Kebuladze, Long-term effects of polyacrylamide hydrogel on human breast tissue, Plast. Reconstr. Surg. 111 (2003) 1883–1890, https://doi.org/10.1097/01.PRS.0000056873.87165.5A.

[31] D. Zhao, J. Huang, Y. Zhong, K. Li, L. Zhang, J. Cai, High-strength and high-toughness double-cross-linked cellulose hydrogels: a new strategy using sequential chemical and physical cross-linking, Adv. Funct. Mater. 26 (2016) 6279–6287, https://doi.org/10.1002/adfm.201601645.

[32] Q. He, Y. Huang, S. Wang, Hofmeister effect-assisted one step fabrication of ductile and strong gelatin hydrogels, Adv. Funct. Mater. 28 (2018), https://doi.org/10.1002/adfm.201705069.

[33] D. Xu, J. Huang, D. Zhao, B. Ding, L. Zhang, J. Cai, High-flexibility, high-toughness double-cross-linked chitin hydrogels by sequential chemical and physical cross-linkings, Adv. Mater. 28 (2016) 5844–5849, https://doi.org/10.1002/adma.201600448.

[34] J.S. Katz, J.A. Burdick, Light-responsive biomaterials: development and applications, Macromol. Biosci. 10 (2010) 339–348, https://doi.org/10.1002/mabi.200900297.

[35] D. Alesa, L. Diniz, J. Otávio, C. Silva, R.M. Ribeiro-costa, A review of the designs and prominent biomedical advances of natural and synthetic hydrogel formulations, Eur. Polym. J. J. 88 (2017) 373–392, https://doi.org/10.1016/j.eurpolymj.2017.01.027.

[36] J. Zhang, W. Xue, Y. Dai, L. Wu, B. Liao, W. Zeng, Double network hydrogel sensors with high sensitivity in large strain range, Macromol. Mater. Eng. (2021) 1–8, https://doi.org/10.1002/mame.202100486, 2100486.

[37] T.E. Brown, K.S. Anseth, Spatiotemporal hydrogel biomaterials for regenerative medicine, Chem. Soc. Rev. 46 (2017) 6532, https://doi.org/10.1039/c7cs00445a.

[38] P.J. Levalley, R. Neelarapu, B.P. Sutherland, S. Dasgupta, C.J. Kloxin, A.M. Kloxin, Photolabile linkers: exploiting labile bond chemistry to control mode and rate of hydrogel degradation and protein release, J. Am. Chem. Soc. 142 (2020) 4671–4679, https://doi.org/10.1021/jacs.9b11564.

[39] M.J. Hansen, W.A. Velema, M.M. Lerch, B.L. Feringa, Wavelength-selective cleavage of photoprotecting groups: strategies and applications in dynamic systems, Chem. Soc. Rev. (2015) 3358–3377, https://doi.org/10.1039/C5CS00118H.

[40] C. Bao, L. Zhu, Q. Lin, H. Tian, Building biomedical materials using photochemical bond cleavage, Adv. Mater. (2015) 1–16, https://doi.org/10.1002/adma.201403783.

[41] A. Romano, I. Roppolo, E. Rossegger, S. Schlögl, M. Sangermano, Recent trends in applying ortho-nitrobenzyl esters for the design of photo-responsive polymer networks, Materials 13 (2020) 12–14, https://doi.org/10.3390/ma13122777.

[42] J.L. Pelloth, P.A. Tran, A. Walther, A.S. Goldmann, H. Frisch, V.X. Truong, C. Barner-kowollik, Wavelength-Selective softening of hydrogel networks, Adv. Mater. 2102184 (2021) 1–9, https://doi.org/10.1002/adma.202102184.

[43] F. Guillier, D. Orain, M. Bradley, Linkers and cleavage strategies in solid-phase organic synthesis and combinatorial chemistry, Chem. Rev. 100 (2000) 2091–2157, https://doi.org/10.1021/cr980040+.

[44] V.N. Rajasekharan Pillai, Photoremovable protecting groups in organic synthesis, Synthesis 1 (1980) 1–26.

[45] Y. Uto, T. Ogata, Y. Kiyotsuka, Y. Miyazawa, Y. Ueno, H. Kurata, T. Deguchi, M. Yamada, N. Watanabe, T. Takagi, S. Wakimoto, R. Okuyama, M. Konishi, N. Kurikawa, K. Kono, J. Osumi, Novel and potent inhibitors of stearoyl-CoA desaturase-1. Part II: identification of 4-ethylamino-3-(2-hydroxyethoxy)-N-[5-(3-trifluoromethylbenzyl)thiazol-2-yl]benzamide and its biological evaluation, Bioorg. Med. Chem. Lett 19 (2009) 4159–4166, https://doi.org/10.1016/j.bmcl.2009.05.123.

[46] L. Li, J.M. Scheiger, P.A. Levkin, Design and applications of photoresponsive hydrogels, Adv. Mater. 31 (2019), https://doi.org/10.1002/adma.201807333.

[47] K. Le, M. Hoang, A. Pardo-vargas, Y. Zhu, Y. Yu, M. Loria, M. Delbianco, P.H. Seeberger, Traceless photolabile linker expedites the chemical synthesis of complex oligosaccharides by automated glycan assembly, J. Am. Chem. Soc. 141 (2019) 9079–9086, https://doi.org/10.1021/jacs.9b03769.

[48] M.C. Koetting, J.T. Peters, S.D. Steichen, A. Nicholas, U. States, U. States, U. States, U. States, U. States, Stimulus-responsive hydrogels: theory, modern advances, and applications, Mater. Sci. Eng. R Rep. 93 (2015) 1–49, https://doi.org/10.1016/j.mser.2015.04.001.Stimulus-responsive.

[49] C.P. Holmes, Model studies for new o-nitrobenzyl photolabile linkers: substituent effects on the rates of photochemical cleavage, J. Org. Chem. 62 (1997) 2370–2380, https://doi.org/10.1021/jo961602x.

[50] D.R. Griffin, A.M. Kasko, Photodegradable macromers and hydrogels for live cell encapsulation and release, J. Am. Chem. Soc. 134 (2012) 13103–13107, https://doi.org/10.1021/ja305280w.

[51] D.R. Griffin, A.M. Kasko, Photoselective delivery of model therapeutics from hydrogels, ACS Macro Lett. 1 (2012) 1330–1334, https://doi.org/10.1021/mz300366s.

[52] M.S. Kim, S.L. Diamond, Photocleavage of o -nitrobenzyl ether derivatives for rapid biomedical release applications, Bioorg. Med. Chem. Lett. 16 (2006) 4007–4010, https://doi.org/10.1016/j.bmcl.2006.05.013.

[53] J. Sun, H. Tan, Alginate-based biomaterials for regenerative medicine applications, Materials 6 (2013) 1285–1309, https://doi.org/10.3390/ma6041285.

[54] J. Sun, H. Tan, Alginate-based biomaterials for regenerative medicine applications, Materials 6 (2013) 1285–1309, https://doi.org/10.3390/ma6041285.

[55] M.M. Pérez-Madrigal, J. Torras, J. Casanovas, M. Häring, C. Alemán, D.D. Díaz, Paradigm shift for preparing versatile m2+-free gels from unmodified sodium alginate, Biomacromolecules 18 (2017) 2967–2979, https://doi.org/10.1021/acs.biomac.7b00934.

[56] T. Lu, Z. Wang, J. Tang, W. Zhang, T. Wang, A pseudo-elasticity theory to model the strain-softening behavior of tough hydrogels, J. Mech. Phys. Solid. 137 (2020), 103832, https://doi.org/10.1016/j.jmps.2019.103832.

[57] R. Bai, J. Yang, X.P. Morelle, C. Yang, Z. Suo, Fatigue fracture of self-recovery hydrogels, ACS Macro Lett. 7 (2018) 312–317, https://doi.org/10.1021/acsmacrolett.8b00045.

[58] W. Zhang, J. Hu, J. Tang, Z. Wang, J. Wang, T. Lu, Z. Suo, Fracture toughness and fatigue threshold of tough hydrogels, ACS Macro Lett. 8 (2019) 17–23, https://doi.org/10.1021/acsmacrolett.8b00788.

[59] R. Bai, J. Yang, Z. Suo, Fatigue of hydrogels, Eur. J. Mech. Solid. 74 (2019) 337–370, https://doi.org/10.1016/j.euromechsol.2018.12.001.

[60] R. Bai, B. Chen, J. Yang, Z. Suo, Tearing a hydrogel of complex rheology, J. Mech. Phys. Solid. 125 (2019) 749–761, https://doi.org/10.1016/j.jmps.2019.01.017.

[61] S. Ponsubha, A.K. Jaiswal, Effect of interpolymer complex formation between chondroitin sulfate and chitosan-gelatin hydrogel on physico-chemical and rheological properties, Carbohydr. Polym. 238 (2020), 116179, https://doi.org/10.1016/j.carbpol.2020.116179.

[62] M. Villiou, J.I. Paez, A. Del Campo, Photodegradable hydrogels for cell encapsulation and tissue adhesion, ACS Appl. Mater. Interfaces 12 (2020) 37862–37872, https://doi.org/10.1021/acsami.0c08568.

[63] Y. Yan, S. Xu, H. Liu, X. Cui, J. Shao, P. Yao, J. Huang, X. Qiu, C. Huang, A multi-functional reversible hydrogel adhesive, Colloids Surf., A 593 (2020), 124622, https://doi.org/10.1016/j.colsurfa.2020.124622.

[64] M.L. Oyen, Mechanical characterisation of hydrogel materials, Int. Mater. Rev. 59 (2014) 44–59, https://doi.org/10.1179/1743280413Y.0000000022.

[65] M. Wang, J. Li, W. Li, Z. Du, S. Qin, Preparation and characterization of novel poly (vinyl alcohol)/collagen double-network hydrogels, Int. J. Biol. Macromol. 118 (2018) 41–48, https://doi.org/10.1016/j.ijbiomac.2018.05.200.

[66] Z. Fan, B. Liu, J. Wang, S. Zhang, Q. Lin, P. Gong, L. Ma, S. Yang, A novel wound dressing based on Ag/graphene polymer hydrogel: effectively kill bacteria and accelerate wound healing, Adv. Funct. Mater. 24 (2014) 3933–3943, https://doi.org/10.1002/adfm.201304202.

[67] K. Lee, E.A. Silva, D.J. Mooney, Growth factor delivery-based tissue engineering: general approaches and a review of recent developments, J. R. Soc. Interface 8 (2011) 153–170, https://doi.org/10.1098/rsif.2010.0223.

[68] M.C. Darnell, J.Y. Sun, M. Mehta, C. Johnson, P.R. Arany, Z. Suo, D.J. Mooney, Performance and biocompatibility of extremely tough alginate/polyacrylamide hydrogels, Biomaterials 34 (2013) 8042–8048, https://doi.org/10.1016/j.biomaterials.2013.06.061.

[69] M.P. Ribeiro, A. Espiga, D. Silva, P. Baptista, J. Henriques, C. Ferreira, J.C. Silva, J.P. Borges, E. Pires, P. Chaves, I.J. Correia, Development of a new chitosan hydrogel for wound dressing, Wound Repair Regen. 17 (2009) 817–824, https://doi.org/10.1111/j.1524-475X.2009.00538.x.

[70] F.M. Carvalho, P. Lopes, M. Carneiro, A. Serra, J. Coelho, A.T. De Almeida, M. Tavakoli, Nondrying, sticky hydrogels for the next generation of high-resolution conformable bioelectronics, ACS Appl. Electron. Mater. 2 (2020) 3390–3401, https://doi.org/10.1021/acsaelm.0c00653.

[71] C.M. Tringides, N. Vachicouras, I. De Lázaro, H. Wang, A. Trouillet, B.R. Seo, A. Elosegui-artola, F. Fallegger, Y. Shin, C. Casiraghi, K. Kostarelos, S.P. Lacour, D.J. Mooney, Viscoelastic surface electrode arrays to interface with viscoelastic tissues, Nat. Nanotechnol. 16 (2021) 1019–1029, https://doi.org/10.1038/s41565-021-00926-z.

[72] R. Green, Elastic and conductive hydrogel electrodes, Nat. Biomed. Eng. 3 (2019) 9–10, https://doi.org/10.1038/s41551-018-0342-7.